J Nanopart Res (2015) 17:270
DOI 10.1007/s11051-015-3072-8

RESEARCH PAPER

Amino acid-catalyzed seed regrowth synthesis of photostable high fluorescent silica nanoparticles with tunable sizes for intracellular studies

Shakiba Shahabi · Laura Treccani · Kurosch Rezwan

Received: 26 February 2015 / Accepted: 6 June 2015 / Published online: 18 June 2015

Abstract Size-controlled fluorescence silica nanoparticles (NPs) are widely used for nanotoxicological studies, and diagnostic and targeted therapies. Such particles can be easily visualized and localized within cell environments and their interactions with cellular components can be monitored. We developed an amino acid-catalyzed seed regrowth technique (ACSRT) to synthesize spherical rhodamine-doped silica NPs with tunable sizes, low polydispersity index as well as high labeling efficiency and enhanced fluorescence photostability. Via ACSRT, fluorescent silica NPs can be obtained by introducing the fluorophore in seed formation step, while a precise control over particle size can be achieved by simply adjusting the concentration of reactants in the regrowth step. Unlike the conventional methods, the proposed ACSRT permits the synthesis of fluorescent silica NPs in a water-based system, without the use of any surfactants and co-surfactants. By this approach, additional linkers for covalent coupling of the fluorophore to silica matrix can be omitted, while a remarkable doping efficiency is achieved. The suitability of these particles for biomedical application is demonstrated by in vitro tests with normal and malignant bone cells. We show that the particles can be easily and unambiguously visualized by a conventional fluorescence microscope, localized, and distinguished within intracellular components. In addition, it is presented that the cellular uptake and cytotoxic profile of silica NPs are strongly correlated to the particle size, concentration, and cell line. The results of in vitro experiments demonstrate that tunable fluorescent silica NPs synthesized with ACSRT can be potentially used for toxicological assessments and nanomedical studies.

Keywords Fluorescence · Nanotoxicology · Osteoblast · Osteosarcoma · Seeds regrowth · Silica nanoparticle · Nanomedicine · Environmental and health effects

S. Shahabi · L. Treccani (✉) · K. Rezwan
Advanced Ceramics, University of Bremen, Am Biologischen Garten 2, 28359 Bremen, Germany
e-mail: treccani@uni-bremen.de

Introduction

In the last years, fluorescent nanomaterials have enabled the design of more rapid, highly sensitive, and easy-to-use tools for in vitro biological assays, clinical diagnosis, and nanomedicine as well as in vivo real-time imaging. Silica-based fluorescent NPs are highly attractive for a broad spectrum of applications, such as biosensing (Hornig and Biskup 2008; Latterini and Amelia 2009), bioimaging (Kumar et al. 2008; Liong et al. 2008; Qian et al. 2008), targeting (Tansub et al. 2012; Tao et al. 2011), drug delivery (Febvay et al. 2010; Rosenholm et al. 2010), DNA carriers (Fuller et al. 2008; Xia et al. 2009), bioassays (Jia et al. 2009), and nanotoxicological risk assessments (Al-Rawi et al. 2011). Indeed, silica particles have many

advantages such as chemical stability, biocompatibility (Gao et al. 2009), optical transparency (Peng et al. 2007), and colloidal stability in aqueous and physiological solutions (He et al. 2012; Nakamura et al. 2007). Moreover, silica NPs can be easily functionalized and allow the conjugation of specific ligands and receptors (Labéguerie-Egéa et al. 2011). In the silica matrix, a large number of organic or inorganic dyes can be hosted and an enhanced photostability as well as low photobleaching and dye leakage can be generated (Guo et al. 2013).

Silica NPs can be synthesized by different methods. The Stöber (Stöber et al. 1968) and the reverse water-in-oil reverse microemulsion (WORM) methods (Bagwe et al. 2004; Nooney et al. 2009) are the most widely used synthesis routes. The Stöber method is based on hydrolysis and condensation reactions of tetraethyl orthosilicate (TEOS) in ethanol with water and employs ammonia as a base catalyst. The Stöber is relative simple, but the particles are neither monodisperse nor exhibit uniformity (Gao et al. 2009; Yokoi et al. 2009). On the contrary, the reverse water-in-oil microemulsion method allows the synthesis of highly monodisperse particles with controllable size (Bagwe et al. 2004; Gao et al. 2007). Nevertheless, the high amounts of surfactants and co-surfactants are used and extensive subsequent time-consuming cleaning steps are mandatory (Finnie and Bartlett 2007). Irrespective of the applied synthesis pathway, widely employed fluorophores such as rhodamine and fluorescein are typically incorporated into silica covalently using an amine-containing silane reagent like 3-aminopropyl triethoxysilane (APTES) as crosslinker (van Blaaderen and Vrij 1992). Although the formation of this linkage is feasible and well studied, some drawbacks have been reported. Due to the competitive hydrolysis and condensation of TEOS and APTES, doping efficiency (DE) of the dyes is usually low (ca. 10 %) in this method (Liang et al. 2013). Moreover, an excess amount of APTES, which is typically used to incorporate the highest possible number of fluorophore molecules into particle, can be co-condensed with TEOS (Ha et al. 2009). Therefore, the amount of final amino terminal groups on the NP surface, which is not reproducibly controllable, can further affect the size uniformity (Nakamura et al. 2007). Furthermore, cytotoxic behavior of APTES-conjugated NPs has been documented (Nan et al. 2008). Considering these limitations, it is desired to develop new synthesis routes to prepare fluorescent silica NPs without using APTES.

A more recent synthesis route for the preparation of highly monodisperse silica NPs is the two-pot seed regrowth technique using basic amino acids like L-lysine and L-arginine as catalysts (Hartlen et al. 2008; Watanabe et al. 2011; Yokoi et al. 2010, 2009). Via the amino acid-catalyzed seed regrowth technique (ACSRT), silica NPs can be synthesized based on the reaction in an emulsion containing water, basic amino acid, and TEOS. The hydrolysis of TEOS takes place at the interface between the water (basic amino acid and water) and oil (TEOS) phases (Watanabe et al. 2011) at weakly basic conditions (pH 9–10). Preformed silica particles act as seed for further particle growth, while new particle formation is suppressed (Watanabe et al. 2011). The role of L-arginine used as the catalyst is of particular interest in the respect of bioinspired chemistry (Yokoi et al. 2009), in comparison to the Stöber and the WORM methods, in which the addition of ammonia serves as catalyst. Moreover, in contrast to the WORM, no surfactant or co-surfactant is used in ACSRT.

Here, a simple route for the synthesis of highly fluorescent silica NPs with well-controllable and tunable size based on the ACSRT is presented. Besides the amino acid, water, and TEOS, we introduce fluorophore molecules in the nucleation step, to form fluorescent silica seeds (referred to as labeled seeds). The water-soluble and photostable organic fluorophore, rhodamine B isothiocyanate (RBITC), was directly incorporated into the seeds without covalent binding. It suggests that this synthesis route eliminates the need for pre-modification and APTES-conjugation of dye. Subsequently, during the regrowth step, labeled seed/SiO_2 particles with sizes from 30 to 90 nm and narrow size distribution were synthesized. Particle size was finely adjusted by carefully controlling the reaction parameters and the proportion of reactants (seeds and TEOS) in the stage of regrowth. The obtained fluorescent NPs were characterized using scanning electron microscopy (SEM), dynamic light scattering (DLS), and fluorescence spectrometry. In addition, their photostability was evaluated by measurement of their photobleaching and photoleaching.

The applicability of these particles for biological studies was assessed by in vitro cell tests with normal (osteoblast; HOB) and malignant (osteosarcoma; MG-

63) bone cell lines. Three particle types with diameters of 30, 59, and 91 nm were used. Their effects on cellular viability and possible cytotoxic damages were studied by a water-soluble tetrazolium salt (WST-1) and lactate dehydrogenase (LDH) assays, respectively. In addition, size- and concentration-dependent cellular uptake and localization were characterized using fluorimetry and fluorescence microscopy.

Materials and methods

Chemicals

For particle synthesis, tetraethyl orthosilicate (TEOS, >99 %, lot no. BCBK1670V), L-arginine (>98 %, lot no. MKBH2770V), rhodamine B isothiocyanate (RBITC, mixed isomers, lot no. MKBJ9031V), and absolute ethanol (>98 %, lot no. SZBB1570V) were obtained from Sigma-Aldrich (Germany) and used as received.

Cell culture tests were carried with human osteoblast cells (HOB, passage 4, lot no. 232R020412, Provitro, Germany) and human osteosarcoma cells (MG-63, passage 98, lot no. 2006399, ATCC, Germany). Dulbecco/Vogt modified Eagle's minimal essential medium (D-MEM, high glucose, lot no. 1206393), antibiotic–antimycotic (lot no. 1209917), Alexa Fluor® 488 phalloidin (AF488, 2U/ml, lot no. 1151587), and LysoTracker® (DND-22, lot no. 791512) were from Invitrogen (Germany). Fetal calf serum (FCS, lot no. 010M3395), paraformaldehyde (PFA, lot no. 53260), phosphate-buffered saline (PBS, lot no. SLBF5741V), Triton ™ X-100 (lot no. MKBL5839V), sodium chloride (NaCl, lot no. 038K00451), and DAPI (0.5 μg/ml, lot no. 1242642) were supplied by Sigma-Aldrich (Germany). WST-1 cell proliferation assay (lot no. 14310400, Roche Diagnostics GmbH, Germany) and LDH Pierce ™ assay (lot no. OL17881450, Thermo Scientific, Germany) were purchased from the suppliers as specified. Double deionized water (ddH_2O) with a conductivity < 0.4 μS cm^{-1} was obtained from an ultrapure water system (Synergy, Millipore, USA) and used for all experiments.

Preparation of labeled seed

The synthesis of labeled seeds of 7 nm size is schematically illustrated in Fig. 1. Briefly, L-arginine was dissolved in 16.9 ml ddH_2O at the concentration of 0.006 M and stirred thoroughly at room temperature. Afterwards, 500 μl of RBITC dissolved in water (0.01 M) was added to the L-arginine solution. The mixture was stirred for 10 min and then heated up to 70 °C, before TEOS addition. The molar composition of the reactants was adjusted to 1:0.02:0.001 of TEOS:L-arginine:RBITC. The mixture was heated in an oil bath at 70 °C for 24 h under magnetic stirring with the rate of 400 rpm. Finally, the dispersion containing labeled silica seeds was used as stock for the regrowth step. The synthesis was carried out in the dark to minimize photobleaching of the fluorescent dye.

Regrowth of labeled seeds

To regrow the labeled seeds to a desired size (Fig. 1), first L-arginine was dissolved in the mixture of water and ethanol with the volume ratio of 1:4 at room temperature. Subsequently, depending on the final expected particle size (Table 1), an appropriate portion of labeled seeds was added to the L-arginine solution. The mixture was stirred for 10 min before heating up to 70 °C. Thereafter, an adequate amount of TEOS according to Table 1 was added. The suspension was then kept at a constant stirring rate of 400 rpm and temperature of 70 °C for 24 h in the dark. Eight different types of NPs with different sizes were prepared only by varying the volume of labeled seeds or added TEOS during the regrowth (Table 1), while the other parameters including pH, temperature, stirring rate, time, L-arginine concentration, and volume ratio water/ethanol were kept constant.

Particle characterization

The SEM images of labeled seed/SiO_2 NPs were taken with a Supra 40 (Carl Zeiss, Oberkochen, Germany) operated at 2.00 kV. No conductive coating was deposited on the particles.

The particle sizes of the labeled seed/SiO_2 NPs were measured using DLS with a Delsa™ Nano C photospectrometer (Beckman Coulter, Brea, CA). The average size d_{50}, polydispersity index (PDI), and standard deviation were obtained from three independent measurements of aqueous dispersions of NPs (5×10^{-3} vol%).

Zeta potential of NPs dispersions in ddH_2O (5×10^{-3} vol%) was measured using Delsa™ Nano

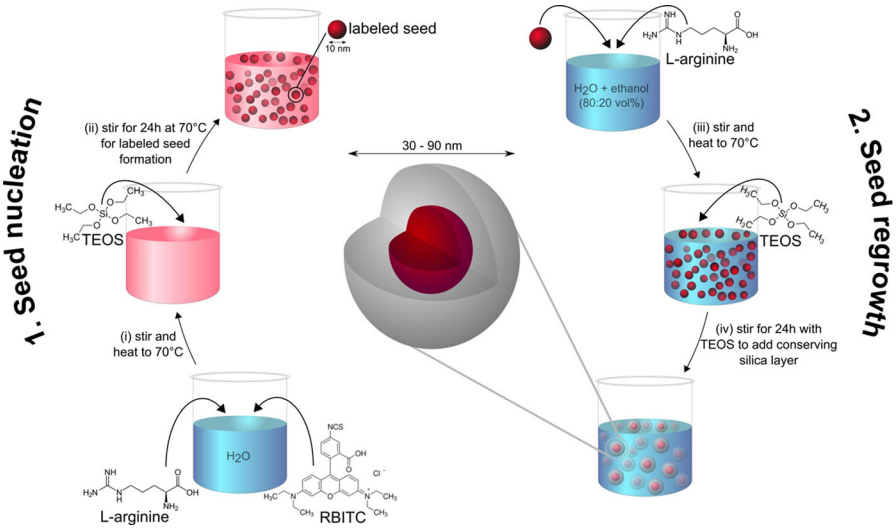

Fig. 1 Schematic illustration of two-pot synthesis of labeled seed/SiO_2 NPs via ACSRT, including seed nucleation and regrowth

Table 1 Composition of labeled seeds and TEOS for the synthesis (in regrowth), diameter determined by SEM and DLS, polydispersity index (PDI), zeta potential of labeled seed/SiO_2 NPs in H_2O and at pH 3.5, quantum yield (φ) values and labeling efficiencies

Sample	Volume of labeled seed in regrowth (ml)	Volume of TEOS in regrowth (ml)	Diameter (SEM) (nm)	Diameter (DLS) (nm)	PDI	ζ Potential in H_2O (mV)	ζ Potential in H_2O (PH 3.5) (mV)	φ	Label efficiency (%)
1a	1	0.5	39 ± 3	67 ± 6	0.07	−39.2 ± 2.8	−23.4 ± 1.7	0.31	71
1b	1	1	47 ± 2	79 ± 4	0.15	−36.5 ± 3.4	−24.3 ± 2.5	0.33	77
1c	1	2	59 ± 3	94 ± 8	0.12	−36.8 ± 1.6	−25 ± 2.9	0.28	75
1d	1	3	91 ± 8	137 ± 16	0.19	−33.3 ± 2.5	−26.4 ± 3.1	0.24	78
2a	2	0.5	30 ± 2	56 ± 5	0.05	−42.1 ± 3	−27.6 ± 2.4	0.38	64
2b	2	1	44 ± 3	69 ± 6	0.09	−38.7 ± 0.8	−24.5 ± 1.2	0.33	65
2c	2	2	52 ± 2	82 ± 5	0.16	−38.4 ± 2.2	−23.9 ± 1.6	0.34	70
2d	1	3	82 ± 7	124 ± 12	0.16	−35.9 ± 1.3	−25.3 ± 2.3	0.28	70

Please note that the compositions of all components in nucleation were kept constant. In regrowth, only the concentrations of labeled seed and TEOS were varied, while the compositions of H_2O, ethanol, and L-arginine were not changed for all eight NPs

C photospectrometer. The same measurement was performed in ddH_2O at PH 3.5. The average value and standard deviations of three measurements were stated.

The UV–Vis absorption and fluorescence spectra at room temperature were obtained by using a multiscan GO spectrophotometer (Thermo Scientific, Finland) and a LS 50 spectrometer (Perkin Elmer, Germany), respectively. Fluorescence spectra of NPs were recorded using aqueous dispersions at the slit widths of 10 and 5 nm for excitation and emission, respectively. In addition, the relative fluorescence quantum yield (φ) of NPs was calculated using dilute methanol solution of Rhodamine 6G ($\varphi = 0.94$) as the standard (Bäumler and Penzkofer 1990), for which the absorbance was kept below 0.2 at the excitation wavelength. Labeling efficiencies are defined as the fraction of added dye molecules actually incorporated in the NPs (Imhof et al. 1999) using the obtained UV–Vis standard curve for RBITC.

To evaluate the photobleaching of the labeled seed/SiO_2 NPs, their fluorescence intensity (FI) was measured after 60 times excitation (once per minute) at 550 nm. Free RBITC dissolved in ddH_2O at the concentration of

10^{-6} M was used as reference. Emission spectra were recorded at each time of excitement. Information about the photostability of NPs and RBITC was obtained by observing their normalized FI versus the excitation time.

The photoleaching of labeled seed/SiO_2 NPs was determined for up to 3 days by incubating their aqueous dispersions (5×10^{-2} vol%) in a cell incubator at 37 °C, 10 % CO_2, and 95 % relative humidity (RH). These conditions were also applied for cell culture experiments with the cells as later described. For each day, 4 replicates from each type of labeled seed/SiO_2 NPs were prepared. The leakage of RBITC from NPs in water was investigated by measuring the FI of supernatant. The supernatants at day 1, 2, and 3 were obtained by centrifugation of the labeled seed/SiO_2 NPs dispersions for 10 min at 2100 g. FI of supernatants at each day represents the photoleaching and was calculated as percent of FI of the respective particle dispersion at the same day.

Cell culture experiments

Cell culturing

In vitro tests were performed with osteoblast and osteosarcoma cells as described in Holthaus et al. (2012). Briefly, the cells were cultured in D-MEM supplemented with 10 % heat-inactivated FCS and 1 % antibiotic–antimycotic in a cell incubator (C200, Labotect Labor-Technik-Göttingen GmbH, Germany) at 37 °C, 10 % CO_2, and 95 % RH. Cells were cultured in cell culture flasks (75 cm^2) for up for 1 week and the medium was renewed every 2 days. Cells were trypsinized and seeded at a density of 2.5×10^4 cells/ml medium onto 15 mmØ Thermanox® coverslips (NUNC, Fischer Scientific, Germany) placed in wells of a 24-well polystyrene multidish (NUNC, Fischer Scientific, Germany). Cells were incubated at 37 °C, 10 % CO_2, and 95 % RH overnight. Dispersions of labeled seed/SiO_2 NPs (30, 59, and 91 nm) were added to the cell medium to final concentrations of 50, 100, and 200 µg/ml. As control, HOB and MG-63 cells with the same density were incubated in the absence of NPs.

Determination of cell viability

The viability of the cells was evaluated using the WST-1 assay. After 4 and 24 h exposure, 100 µl of WST-1 cell proliferation reagent was added to the culture wells and incubated for 2 h at 37 °C, 10 % CO_2, and 95 % RH. Thereafter, the cell medium was centrifuged for 5 min at 20000×*g* to remove the NPs. Supernatants were quantified spectrometrically using multiscan GO spectrophotometer (Thermo Scientific, Finland) at 450 nm with a reference wavelength of 650 nm.

The cellular and extracellular activity of the cytosolic enzyme LDH was quantified using the LDH assay as described in Dringen et al. (Dringen et al. 1998). After each sampling point, the media were collected from each well and centrifuged for 5 min at 20000×*g* to separate the NPs before the measurement of extracellular LDH. For quantification of cellular LDH, the cells were afterwards rinsed with PBS buffer, trypsinized, and analyzed. 50 µL of media or cell lysates was used in the assay and measured using the multiscan GO spectrophotometer. The percent of either extracellular or cellular LDH activity was calculated by dividing the measured amount by the total activity (medium plus lysate).

Quantification of cellular uptake of NPs

To estimate particle uptake by HOBs and MG-63, the cells were trypsinized and washed with PBS three times with centrifugation for 5 min at 12,000×*g*. Subsequently, the cell pellet was resuspended in PBS and analyzed by fluorimetry in black well plates (Greiner Bio-One, Germany) using a microplate reader (Chameleon, HIDEX, Turku, Finland) at the excitation wavelength of 544 and emission of 590 nm. Data are expressed as FI units after subtracting background (cells without NPs) and normalizing to the FI of labeled seed/SiO_2 NPs dispersions, which were measured under the same conditions as cell pellets.

Statistical analysis

The results of WST-1 assay, LDH activity, and quantification of cellular uptake were expressed as mean ± standard deviation of three independent experiments. The statistical analysis was performed using the software Minitab 16 (Minitab Inc., Pennsylvania). The data were subjected to one-way analysis of variance (ANOVA) followed by Dunnett's method for multiple comparisons, and p values of less than 0.05 ($p < 0.05$) were considered to be statistically significant.

Cell staining and imaging

After 4 and 24 h exposure to NPs at a concentration of 200 μg/ml, HOB and MG-63 cells were fixed with PFA and fluorescently stained with DAPI for the cell nuclei and AF488 for actin cytoskeletons. NPs uptake and distribution within the cells were analyzed using an AX-10 fluorescence microscope (Zeiss, Germany). Particle co-localization within lysosomes was determined with the LysoTracker®. 75 nM LysoTracker® was applied at the last hour of the incubation time with NPs. Thereafter, the cells were washed twice with PBS and fixed with PFA. Cell cytoskeleton was stained with AF488. Labeled seed/SiO_2 NPs appeared red, lysosomes blue, and actin cytoskeletons green.

Results and discussion

Particle characterization

In this study, an amino acid-catalyzed seed regrowth method was used for the synthesis of fluorescently labeled silica NP with controllable size and high fluorescence. L-arginine was applied as catalyst and fluorescent dye molecules were incorporated directly (without APTES-conjugation) into the particle nuclei formed by hydrolysis and condensation of TEOS. Particle regrowth was achieved in the second step due to the polymerization of TEOS. Synthesized fluorescent silica NPs were characterized via different methods prior to in vitro test.

SEM and DLS analyses are shown in Fig. 2a, b. The NP diameter obtained from SEM images, the mean hydrodynamic particle sizes (d_{50}) by DLS, PDI, and zeta potential values are summarized in Table 1. SEM micrographs showed that the synthesized labeled seed/SiO_2 NPs had a spherical shape and a narrow size distribution. DLS measurements confirmed low PDI for all labeled seed/SiO_2 NPs. A high control of the NP size between about 30 and 90 nm was obtained only by proportionally varying the concentrations of two components in regrowth step including added labeled seeds and TEOS. In our approach, we showed that by using a constant volume of labeled seeds in regrowth step, the particle size can be systematically increased by increasing TEOS concentration. We noticed also that the final particle size depended on the amount of labeled seeds employed in the regrowth. More labeled seeds were introduced during regrowth, and the final diameter of the as-prepared NPs was found to be small. It could be attributed to the rates of hydrolysis of TEOS and condensation of silicate species, as the solubility of silicate species is extremely sensitive to the synthesis system under the weakly basic conditions (pH 9–11) (Brinker and Scherer 1990). Hence, slight changes in the composition at the regrowth stage can strongly influence the production rate of silicate species (Watanabe et al. 2011). The change in the amount of TEOS as a silica source would cause the change in the concentration of the silicate species, leading to the changes in the size of the final particles (Yokoi et al. 2009). In each image, almost no differently sized NPs were observed. This strongly suggested that the added TEOS in the regrowth stage contributed only to the resumed growth of the seeds, not to the formation of new silica particles (Watanabe et al. 2011). The volume of added TEOS was selected precisely that it almost completely consumed for regrowth of the existed labeled seeds rather than generation of new ones. Moreover, different NPs only varied in size and not in shape.

The zeta potentials of the NPs in ddH_2O were quite similar, ranging from −33.3 to −42.1 mV. All labeled seed/SiO_2 NPs showed negative charge between −23.4 and −27.6 mV at pH 3.5. These negative zeta potential values confirmed that the isoelectric point of all labeled seed/SiO_2 NPs was lower than 3.5, as expected for a surface that consists of silica (Parks 1965).

The fluorescence characteristics of the labeled seed/SiO_2 NPs by measurement of their emission spectra at excitation wavelengths of RBITC (550 nm) are shown in Fig. 2c. All NPs featured distinct fluorescence signals but with different intensities. Typically, the fluorescence of dye-doped NPs is proportional to the number of dye molecules used for incorporation in the silica matrix. Higher numbers usually lead to a stronger emission signal except at the concentration limit where self-quenching occurs (Jin et al. 2008). We noticed that intensity at emission peak of NPs depended directly on the amount of labeled seeds, which were used in the synthesis according to the 1. Higher volume of labeled seeds used in the regrowth step, more fluorophore molecules were incorporated in the NPs and stronger FI was measured. Moreover, it was observed that FI systematically increased with decrease of added TEOS in regrowth. Accordingly, smaller NPs presented higher FI, when the volume of

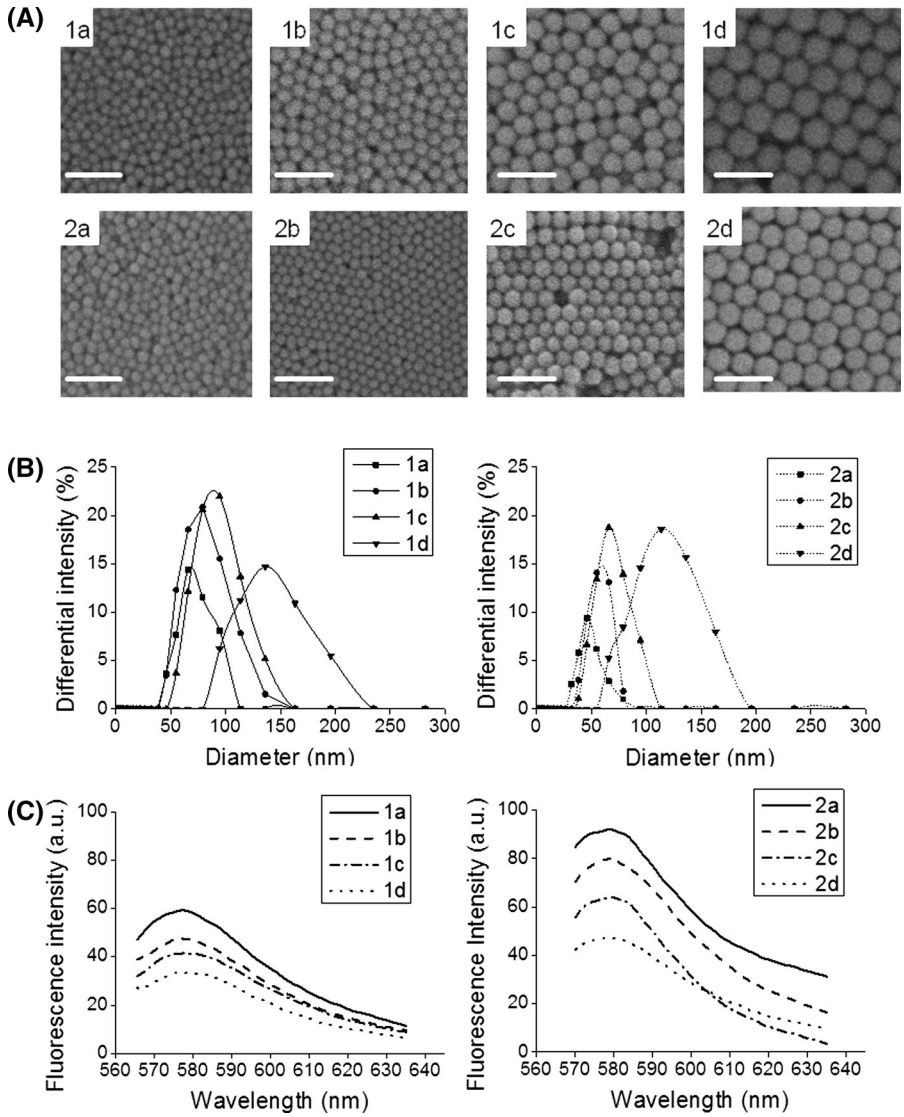

Fig. 2 SEM micrographs (**a**), size distribution obtained by DLS (**b**), and emission spectra of labeled seed/SiO_2 at the excitation wavelength of 550 nm (**c**). The *scale bar* is 200 nm for all SEM images

used labeled seeds in the synthesis was kept constant (Table 1). Because FI of smaller NPs were measured by more number of labeled seeds, which had been used in the regrowth step, compared to larger particles, as the emission spectra of all NPs dispersions were recorded at the same concentration. In addition, in smaller NPs, the labeled seeds are shielded with less silica in comparison to the larger ones.

Quantum yield values ranged between 0.24 and 0.38 (Table 1). This shows that fluorescence efficiency of applied ACSRT is in a comparable range as other typical synthesis methods for fluorescent silica NPs (Kumar et al. 2008; Larson et al. 2008). However, a precise comparison between the quantum yields of NPs, synthesized with ACSRT and other routes, should be further studied, when the same dye and at the similar concentration is used for doping. In addition, the labeling efficiency of the synthesized silica NPs was between 64 and 78 % (Table 1), much higher than that in the conventional coupling routes using APTES (Imhof et al. 1999). The reason responsible for the low labeling efficiency in the other

methods is the competitive hydrolysis and condensation of TEOS and APTES (Liang et al. 2013). Typically the hydrolysis and condensation rates of APTES are much slower than those of TEOS (van Blaaderen and Vrij 1993); therefore, most of the APTES are left in the solution upon the complete condensation of TEOS, resulting of the low DE of the dye (Liang et al. 2013). Our results demonstrated that, via ACSRT, the synthesis of dye-doped silica NPs with high labeling efficiency could be achieved without using APTES.

To assess the photostability, NPs aqueous dispersion and RBITC solution were excited 60 times (once in a minute) at 550 nm. Representative particle photobleaching of aqueous dispersion of sample 2c (5×10^{-2} vol%) and that of free RBITC dissolved in ddH_2O at concentration of 10^{-6} M are presented in Fig. 3a. Evaluation of photostability showed that the fluorescence maxima of the free dye were dependent on the number of excitations in contrast to the NPs, which had stable signal intensity and no photobleaching. It indicates that the dye is encapsulated inside the silica matrix, which provides an effective barrier keeping the dye from the surrounding environment especially from oxygen (Zhao et al. 2004).

The leaching of RBITC from the labeled seed/SiO_2 NPs in ddH_2O was investigated by measuring the FI of supernatant for up to 3 days. Exemplary results of sample 2c are shown in Fig. 3b. NPs showed negligible leakage of RBITC confirming that entrapment of dyes inside silica matrix could effectively help to prevent their leaching after immersion in water (Gao et al. 2007; He et al. 2012).

Cell culture tests with osteoblasts and osteosarcomas

For in vitro experiments, HOB and MG-63 cells were exposed to three NPs with diameters of 30, 59, and 91 nm and to three different concentrations (50, 100, and 200 µg/ml) for 4 and 24 h. Quantification of intracellular FI of labeled seed/SiO_2 NPs, as an indicator for amount of cellular internalization, is illustrated in Fig. 4. From these experiments, dose-dependent uptake of NPs was observed for both cell lines. FI of cell pellets originated from internalized NPs after exposure to 200 µg/ml was significantly higher than lower concentrations (50 and 100 µg/ml), independent of incubation time and type of the cells.

In addition, size-dependent cellular uptake was observed. The NPs with a diameter of 30 nm resulted in a significantly higher uptake with HOB cells after 24 h compared to both larger NPs. Nevertheless, 4 h exposure led to a significant difference between cellular uptake of 30 nm only in comparison to 91 nm, and no evident differences between the intracellular FI from 30 to 59 nm NPs were detected (Fig. 4a). The accumulation of 30 nm labeled seed/SiO_2 in MG-63 cells was significantly higher than 59 and 91 nm NPs, independent of exposure time (Fig. 4b). Our results suggest strongly that smaller NPs were taken up with higher efficiency than larger

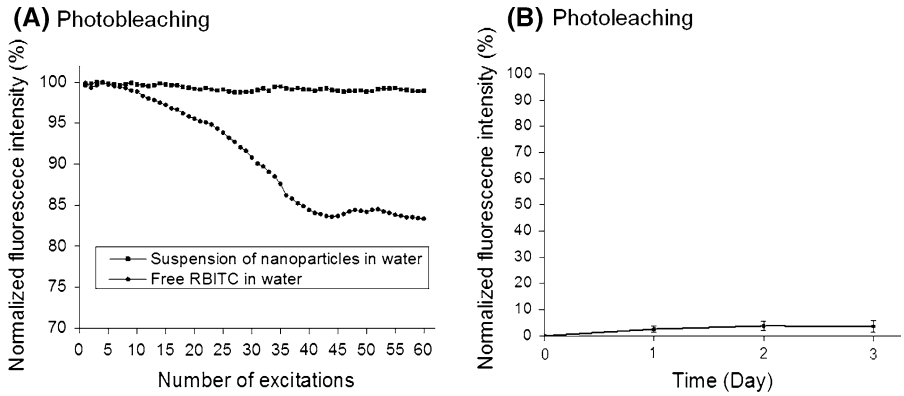

Fig. 3 Fluorescence stability of synthesized labeled seed/SiO_2 including photobleaching measurements of the dispersion of sample 2c in water (5×10^{-2} vol%) and free RBITC in water (10^{-6} M) (**a**) and photoleaching of RBITC from labeled seed/SiO_2 (sample 2c) at 37 °C (**b**). The data are expressed as mean ± standard deviation ($N = 4$) given as the percentage of original FI

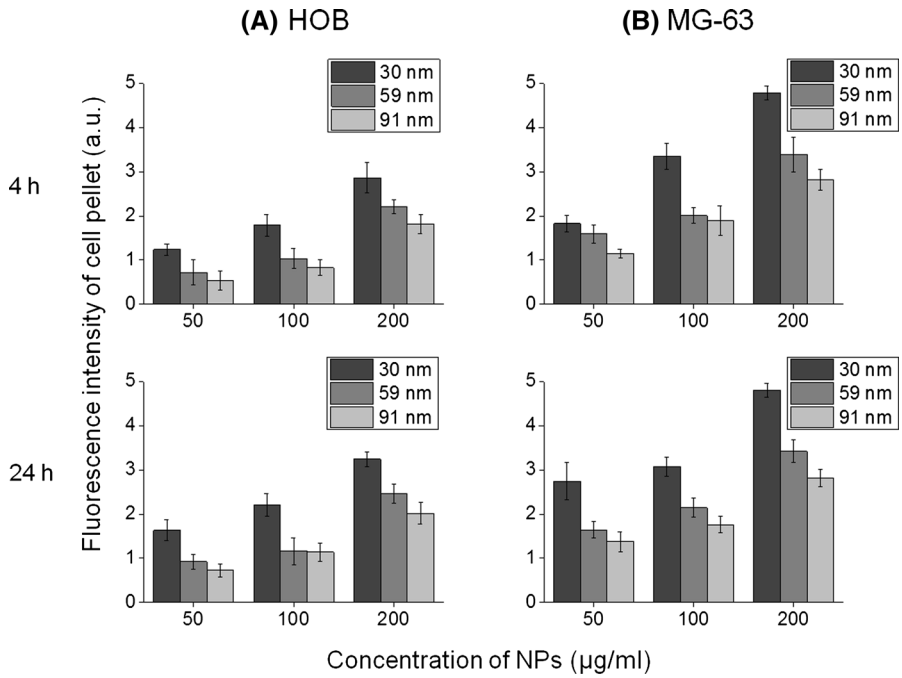

Fig. 4 Intracellular FI of HOB and MG-63 cell pellets representing the cellular uptake of labeled seed/SiO_2 NPs after incubation for 4 and 24 h with the concentrations of 50, 100, and 200 µg/ml. FI of the cell pellets after uptake was measured by fluorimetry and normalized to the intensity of relevant NPs after subtraction of background fluorescence from the control (cells cultured without NPs). The data are expressed as mean ± SD from three independent experiments

sized particles in both cell lines. This observation is consistent with other reports on size dependency of silica NP internalization within the cells (Guarnieri et al. 2014; Lu et al. 2009).

The statistical analysis showed that with all three sizes, the internalization of NPs in MG-63 cells was significantly higher in comparison to that in HOBs. This could be related to higher metabolic activities and shorter doubling time of the osteosarcomas compared to osteoblasts. The MG-63 cells used in our experiments had much shorter cell population doubling time (about 35 h) than HOBs (72 h). The difference between intracellular FI of NPs-treated cells after 4 and 24 h is negligible for both cell lines suggesting that the penetration of NPs into the cells took place mostly at the first hours of exposure.

The interaction and effects of labeled seed/SiO_2 NPs on osteoblasts and osteosarcoma cells were determined by monitoring cell viability using the WST-1 assay. HOB cells' survival rate significantly decreased upon exposure to the NPs with diameter of 30 nm at the highest concentration of 200 µg/ml (Fig. 5a). However, the same NPs at lower concentrations did not strongly disturb HOB viability. Both larger NPs (59 and 91 nm) did not show any discernible effects on osteoblast viability within all ranges of concentrations. Moreover, no significant difference in proliferation of the MG-63 was found after 4 and 24 h incubation with three different sized labeled seed/SiO_2 NPs in comparison to control (Fig. 5b).

To investigate possible cytotoxic effects of labeled seed/SiO_2 NPs on HOB and MG-63 cells, cellular and extracellular LDH activities were assessed after 4 and 24 h incubation with 30, 59, and 91 nm NPs at concentrations of 50, 100, and 200 µg/ml (Fig. 6). A statistically significant increase in LDH leakage after 4 h exposure was observed for HOB cells with 30 nm labeled seed/SiO_2 NPs only at the concentration of 200 µg/ml in comparison to control samples (cells cultivated without NPs) shown in Fig. 6a. Nevertheless, significant cytotoxicity was apparent after 24 h for both 30 and 59 nm at the highest concentration (200 µg/ml). Exposure of osteoblasts to 91 nm silica NPs induced no cytotoxic damages, irrespective of applied exposure time. The absence of any significant increase in extracellular or decrease in cellular LDH activity of MG-63 exposed to particles with different sizes and at different concentrations (Fig. 6b) indicates that the labeled seed/SiO_2 NPs are non-cytotoxic to osteosarcomas.

Our results indicated that exposure to the small- and medium-sized applied silica NPs (30 and 59 nm)

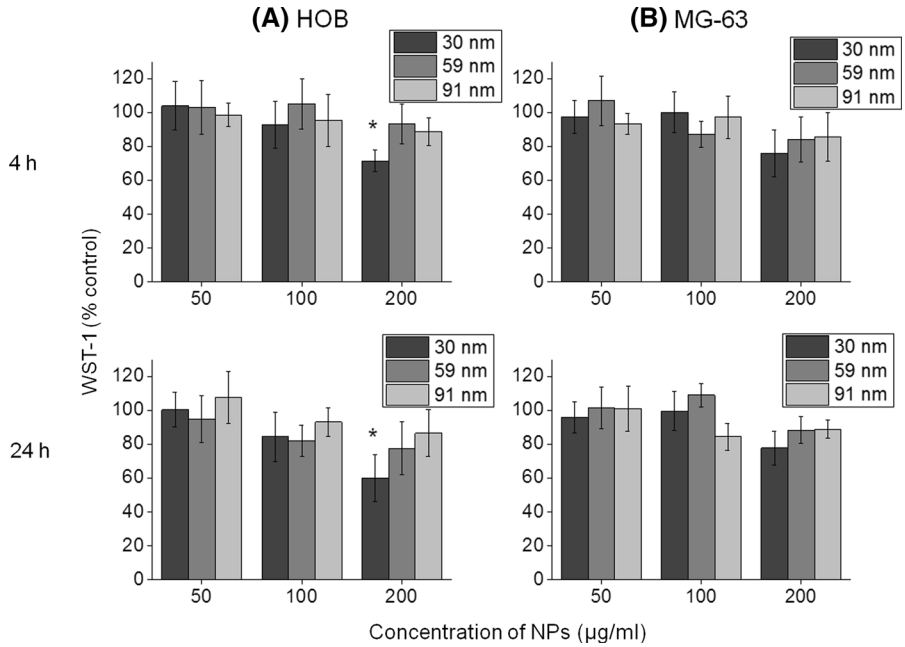

Fig. 5 Influence of labeled seed/SiO_2 NPs with sizes of 30, 59, and 91 nm on the viability of **a** HOB and **b** MG-63 cells after 4 and 24 h at 37 °C, measured by WST-1 assay. The cells were exposed to different concentrations of NPs (50, 100, and 200 μg/ml). The data are expressed as mean ± standard deviation (from three independent experiments) given as the percentage of the control (absence of NPs). *Asterisk* indicates significant differences in comparison to the control ($p < 0.05$)

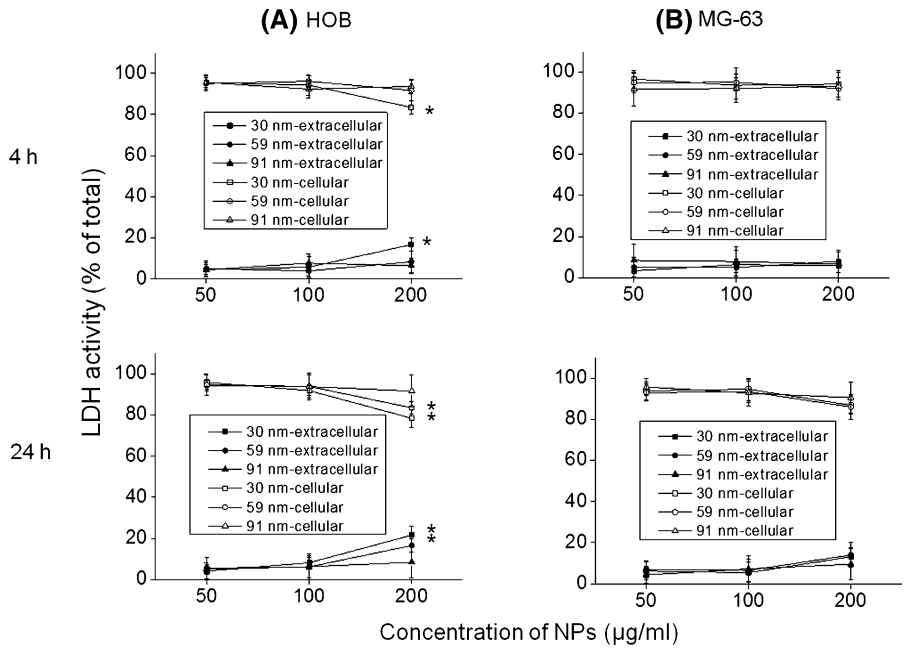

Fig. 6 The cellular and extracellular LDH activities of HOB (**a**) and MG-63 (**b**), exposed to labeled seed/SiO_2 NPs with sizes of 30, 59, and 91 nm at the concentrations of 50, 100, and 200 μg/ml after 4 and 24 h at 37 °C. The data are expressed as mean ± standard deviation from three independent experiments. *Asterisk* indicates significant differences ($p < 0.05$) in comparison to the control (absence of NPs)

induced cytotoxic damages only at the highest applied concentration of 200 μg/ml (Fig. 5a, 6a). This could be attributed to their highest accumulation in the cytoskeletons, which probably hampered the metabolism of the HOB cells (Fig. 4a). This is in agreement with results obtained on osteoblasts exposed to other types of silica NPs (Beck et al. 2012). Interestingly, exposure of MG-63 cells to labeled seed/SiO_2 NPs did not result in significant inhibition of cell viability (as determined by the WST-1 assay, Fig. 5b) and caused no cytotoxic damage (as analyzed by LDH assay, Fig. 6b), irrespective of the size and concentration of NPs or time of exposure. It suggests

that MG-63 cells are more resistant to silica NPs as compared to normal bone cells. The cell population doubling time could be an important factor of the susceptibility of cells exposed to particles. A correlation between cytotoxic effects and the population doubling time of different cell lines treated with silica NPs, including lung, skin, and gastric and colon cells, has been documented (Chang et al. 2007).

The uptake of three different sized labeled seed/SiO_2 NPs after 4 and 24 h exposure was investigated through fluorescence microscope imaging (Fig. 7). Microscopy of HOB and MG-63 cells, treated with labeled seed/SiO_2, indicated that irrespective of size, NPs were visualized to be taken up with both cell types. All three sized NPs are internalized into cytoskeletons of the HOB and MG-63 cells. However, the NPs were not equally distributed within the cells but accumulated mostly with affinity in the central part of the cells and around the nuclei. The microscopy micrographs confirmed that our labeled seed/SiO_2 NPs are detectable with their intense red fluorescence simultaneously with dyes, which were utilized for staining of cell nuclei and actin cytoskeleton, DAPI and AF488, respectively, making labeled seed/SiO_2 NPs an appropriate candidate for use in nanobiological studies.

Moreover, we used fluorescence capacities of labeled seed/SiO_2 NPs for co-localization analysis with lysosomal components. The cells were exposed to the three differently sized NPs and subsequently stained with the LysoTracker® (blue) and then fixed, stained with AF488 for actin cytoskeleton (green), and observed with fluorescence microscopy. No significant differences were observed between the co-localization of NPs after 4 and 24 h exposure. Representative images of the stained cells after 24 h incubation with NPs at 200 μg/ml are shown in Fig. 8. The first column on the left shows merging of three fluorescence microscope channels specific for the LysoTracker® (blue), actin cytoskeleton (green), and labeled seed/SiO_2 NPs (red). The images in the second and third columns reveal the combination of both fluorescences originated from LysoTracker® and NPs. In the second column, the LysoTracker® is shown with its original blue color, which merged to magenta for partial overlapping with red fluorescent NPs. To clarify the combination of both colors of LysoTracker® and NPs and simplify image analysis for co-localization studies, pseudo color micrographs were prepared using the software of fluorescence microscope. The pseudo images (the third column on the left) reveal the lysosomes with green, allowing the observation of the overlapping with the red labeled seed/SiO_2 NPs with yellow color. Overlay of fluorescences from LysoTracker® and NPs, magenta in the

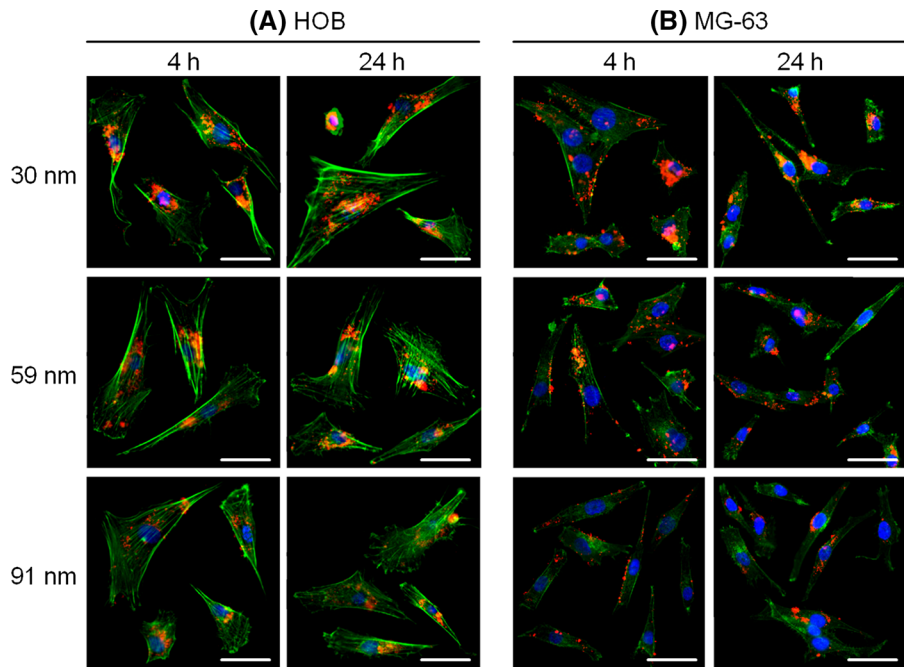

Fig. 7 Fluorescence microscopy images of HOB (**a**) and MG-63 (**b**) cells incubated for 4 and 24 h at 37 °C with 200 μg/ml labeled seed/SiO_2 NPs with the diameters of 30, 59, and 91 nm. The *red* fluorescent NPs can be imaged together with fluorescently labeled cell nucleus (*blue*) and actin cytoskeleton (*green*). *Scale bars* represent 50 μm. (Color figure online)

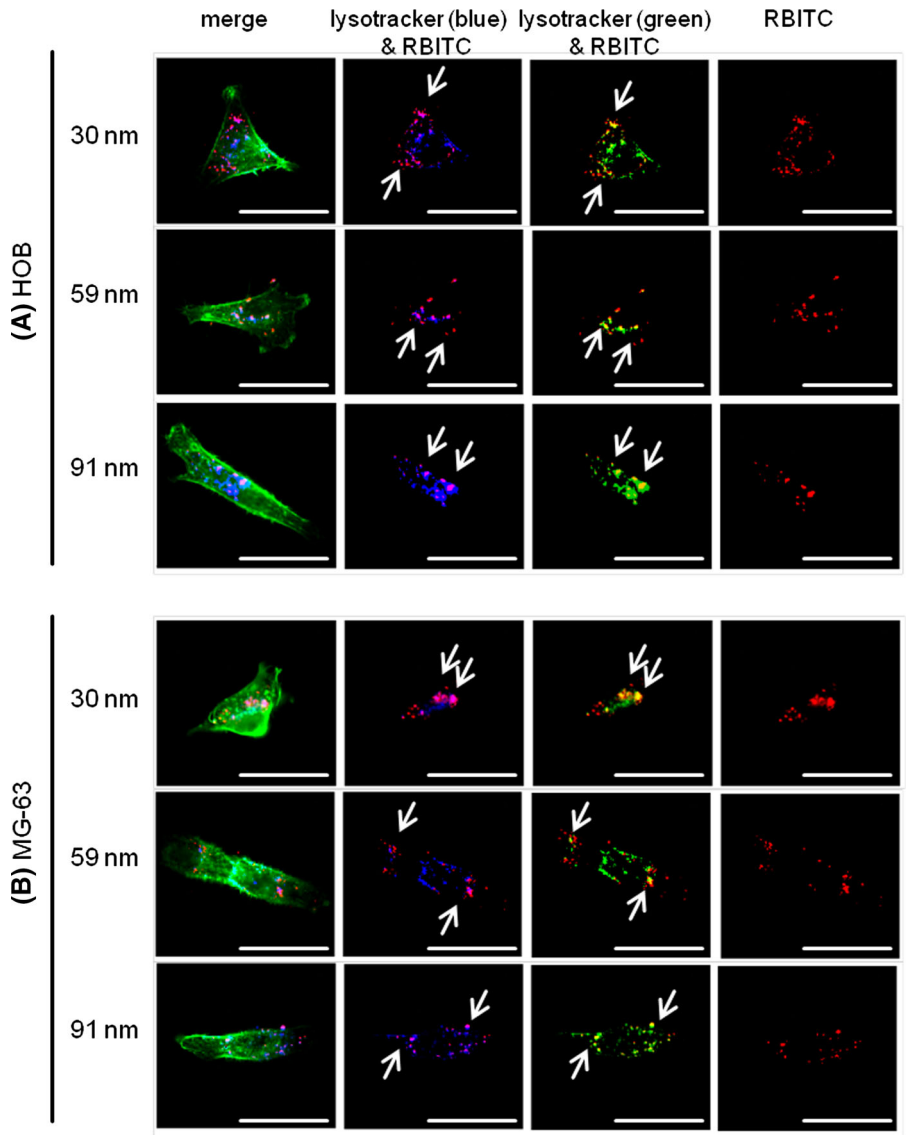

Fig. 8 The lysosomal localization of labeled seed/SiO_2 NPs after incubation of HOB (**a**) and MG-63 (**b**) cells for 24 h at 37 °C with 200 μg/ml of three sized NPs. In the *first column* on the *left*, the merged micrographs of *green* (actin cytoskeletons), *blue* (LysoTracker®), and *red* (RBITC-labeled NPs) are represented. The *second* and *third columns* show the overlay of LysoTracker® and NPs. In the *second column*, the LysoTracker® is visible with its original *blue color*, whereas it is shown with *pseudo green color* in the *third column* to clarify the overlapping with the NPs, which is obvious with the *yellow color*. The *white arrows* denote the intracellular accumulation of labeled seed/SiO_2 NPs within endo-lysosomes of HOB and MG-63 cells. In the *right column*, fluorescently labeled seed/SiO_2 NPs are observed with the single *red* channel. The *scale bars* represent 50 μm. (Color figure online)

second and yellow in the third column, respectively, which are indicated with white arrows, demonstrates the intracellular accumulation of NPs inside the endo-lysosomes. This suggests that endocytotic processes are likely involved in the uptake of three sized labeled seed/SiO_2 NPs into both HOB and MG-653 cells. This is consistent with other reports, which show that silica NPs were visualized in lysosomes of different cell lines (Al-Rawi et al. 2011; Lu et al. 2007; Shi et al. 2010; Zhao et al. 2009).

Our results obtained from characterization of labeled seeds/SiO_2 NPs and in vitro test suggest that

the synthesized particles with strong fluorescence amplitude, high photostability, and enhanced biocompatibility can be employed in variety of nanomedical applications. For instance, we recently used them successfully for the synthesis of bifunctional submicron colloidosomes, co-assembled with superparamagnetic NPs (Bollhorst et al. 2014).

Conclusion

We presented a bioinspired feasible method for synthesis of photostable fluorescent silica NPs with high labeling efficiency, spherical shape, and narrow size distribution based on ACSRT. Fluorophore molecules were incorporated directly in the seeds without using additional crosslinker like APTES. Our results demonstrated that tuning of the particle sizes in the range of about 30–90 nm was accomplished. The size and FI of final labeled seed/SiO_2 NPs could be tailored by precisely controlling the proportion of the added labeled seeds and TEOS during the regrowth step.

Our in vitro studies confirm that fluorescent silica NPs synthesized via ACSRT could be successfully visualized within the cells, co-localized with cellular components, and analyzed via fluorimetry, due to their strong fluorescence amplitude. The presented results clearly demonstrate that the internalization and possible cytotoxicity of silica NPs within the cell greatly depend on the particle size, concentration, and the type of cell (normal versus malignant). Small- and medium-sized labeled seed/SiO_2 NPs (30 and 59 nm) partially compromised viability of normal bone cells only at the highest applied dosage (200 μg/ml), whereas no induced cytotoxic damage was observed at the lower concentrations. In contrast, under our experimental conditions, the proliferation of malignant bone cells did not significantly change after exposure to three sized silica NPs at all applied dosages. Clearly, further studies are needed to address details of cellular uptake and different endocytotic pathways of silica particles into HOB in comparison to MG-63 cells. Our results strengthen the idea that the synthesized fluorescent SiO_2 NPs have a high cellular labeling efficiency as well as a high potential for tracking in vitro occurrences of bone cells. Moreover, since biofunctionalization of silica is well documented, labeled seed/SiO_2 would be a promising approach and versatile platform in many biotechnological applications after conjugation to targeting agents.

Acknowledgments We greatly thank Dr. Jan Köser of Zentrale Analytik, University of Bremen for DLS measurements, Eike Volkmann and Tobias Bollhorst of Advanced Ceramics, University Bremen for helping with statistical analysis and for scientific discussion, respectively. This work was supported by the European Research Council within the SIRG Project "BiocerEng" Project No. 205509.

References

Al-Rawi M, Diabate S, Weiss C (2011) Uptake and intracellular localization of submicron and nano-sized SiO_2 particles in HeLa cells. Arch Toxicol 85:813–826

Bagwe R, Yang C, Hilliard L, Tan W (2004) Optimization of dye-doped silica nanoparticles prepared using a reverse microemulsion method. Langmuir 20:8336–8342

Bäumler W, Penzkofer A (1990) Fluorescence spectroscopic analysis of N and P isomers of DODCI. Chem Phys 140:75–97

Beck G Jr, Ha S, Camalier C, Yamaguchi M, Li Y, Lee J, Weitzmann M (2012) Bioactive silica-based nanoparticles stimulate bone-forming osteoblasts, suppress bone-resorbing osteoclasts, and enhance bone mineral density in vivo. Nanomedicine 8:793–803

Bollhorst T, Shahabi S, Wörz K, Petters C, Dringen R, Maas M, Rezwan K (2014) Bifunctional submicron colloidosomes co-assembled from fluorescent and superparamagnetic nanoparticles. Angew Chem 127(1):120–125

Brinker C, Scherer G (1990) Sol–gel science. Academic Press, New York

Chang J-S, Chang K, Hwang D-F, Kong Z-L (2007) In vitro cytotoxicitiy of silica nanoparticles at high concentrations strongly depends on the metabolic activity type of the cell line. Environ Sci Technol 41:2064–2068

Dringen R, Kussmaul L, Hamprecht B (1998) Detoxification of exogenous hydrogen peroxide and organic hydroperoxides by cultured astroglial cells assessed by microtiter plate assay. Brain Res Protoc 2:223–228

Febvay S, Marini D, Belcher A, Clapham D (2010) Targeted cytosolic delivery of cell-impermeable compounds by nanoparticle-mediated, light-triggered endosome disruption. Nano Lett 10:2211–2219

Finnie K, Bartlett J, Barbé C, Kong L (2007) Formation of silica nanoparticles in microemulsions. Langmuir 23:3017–3024

Fuller J, Zugates G, Ferreira L, Ow H, Nguyen N, Wiesner U, Langer R (2008) Intracellular delivery of core-shell fluorescent silica nanoparticles. Biomaterials 29:1526–1532

Gao F, Tang L, Dai L, Wang L (2007) A fluorescence ratiometric nano-pH sensor based on dual-fluorophore-doped silica nanoparticles. Spectrochim Acta Part A 67:517–521

Gao X, He J, Deng L, Cao H (2009) Synthesis and characterization of functionalized rhodamine B-doped silica nanoparticles. Opt Mater 31:1715–1719

Guarnieri D, Malvindi M, Belli V, Pompa P, Netti P (2014) Effect of silica nanoparticles with variable size and surface

functionalization on human endothelial cell viability and angiogenic activity. J Nanopart Res 16:1–14
Guo Y, Li X, Ye S, Zhang S (2013) Modern optical techniques provide a bright outlook for cell analysis. Trends Anal Chem 42:168–185
Ha S-W, Camalier C-E, Beck GR Jr, Lee J-K (2009) New method to prepare very stable and biocompatible fluorescent silica nanoparticles. Chem Commun 20:2881–2883
Hartlen K, Athanasopoulos A, Kitaev V (2008) Facile preparation of highly monodisperse small silica spheres (15 to >200 nm) suitable for colloidal templating and formation of ordered arrays. Langmuir 24:1714–1720
He X, Wang Y, Wang K, Chen M, Chen S (2012) Fluorescence resonance energy transfer mediated large stokes shifting near-infrared fluorescent silica nanoparticles for in vivo small-animal imaging. Anal Chem 84:9056–9064
Holthaus M, Stolle J, Treccani L, Rezwan K (2012) Orientation of human osteoblasts on hydroxyapatite-based microchannels. Acta Biomater 8:394–403
Hornig S, Biskup C, Grä fe A, Wotschadlo J, Liebert T, Mohr G, Heinze T (2008) Biocompatible fluorescent nanoparticles for pH-sensoring. Soft Matter 4:1169–1172
Imhof A, Megens M, Engelberts J, de Lang D, Sprik R, Vos W (1999) Spectroscopy of fluorescein (FITC) dyed colloidal silica spheres. J Phys Chem B 103:1408–1415
Jia T, Cai Z, Chen X, Lin Z, Huang X, Chen X, Chen G (2009) Electrogenerated chemiluminescence ethanol biosensor based on alcohol dehydrogenase functionalized Ru(bpy)3 2 + doped silica nanoparticles. Biosens Bioelectron 25:263–267
Jin Y, Lohstreter S, Pierce D, Parisien J, Wu M, Hall C III, Zhao J (2008) Silica nanoparticles with continuously tunable sizes: synthesis and size effects on cellular contrast imaging. Chem Mater 20:4411–4419
Kumar R et al (2008) Covalently dye-linked, surface-controlled, and bioconjugated organically modified silica nanoparticles as targeted probes for optical imaging. ACS Nano 2:449–456
Labéguerie-Egé AJ, McEvoy H, McDonagh C (2011) Synthesis, characterisation and functionalisation of luminescent silica nanoparticles. Nanopart Res 13:6455–6465
Larson D, Ow H, Vishwasrao H, Heikal A, Wiesner U, Webb W (2008) Silica nanoparticle architecture determines radiative properties of encapsulated fluorophores. Chem Mater 20:2677–2684
Latterini L, Amelia M (2009) Sensing proteins with luminescent silica nanoparticles. Langmuir 25:4767–4773
Liang J, Xue Z, Xu J, Li J, Zhang H, Yang W (2013) Highly efficient incorporation of amino-reactive dyes into silica particles by a multi-step approach. Colloids Surf A 426:33–38
Liong M et al (2008) Multifunctional inorganic nanoparticles for imaging, targeting, and drug delivery. ACS Nano 2:889–896
Lu C-W et al (2007) Bifunctional magnetic silica nanoparticles for highly efficient human stem cell labeling. Nano Lett 7:149–154
Lu F, Wu S-H, Hung Y, Mou C-Y (2009) Size effect on cell uptake in well-suspended, uniform mesoporous silica nanoparticles. Small 5:1408–1413
Nakamura M, Shono M, Ishimura K (2007) Synthesis, characterization, and biological applications of multifluorescent silica nanoparticles. Anal Chem 79:6507–6514
Nan A, Bai X, Son S, Lee S, Ghandehari H (2008) Cellular uptake and cytotoxicity of silica nanotubes. Nano Lett 8:2150–2154
Nooney R, McCahey C, Stranik O, Guevel X, McDonagh C, MacCraith B (2009) Experimental and theoretical studies of the optimisation of fluorescence from near-infrared dye-doped silica nanoparticles. Anal Bioanal Chem 393:1143–1149
Parks G (1965) The isoelectric point of solid oxides, solid hydroxides, and aqueous hydroxo complex systems. Chem Rev 65:177–198
Peng J, He X, Wang K, Tan W, Wang Y, Liu Y (2007) Non-invasive monitoring of intracellular pH change induced by drug stimulation using silica nanoparticle sensors. Anal Bioanal Chem 388:645–654
Qian J, Li X, Wei M, Gao X, Xu Z, He S (2008) Bio-molecule-conjugated fluorescent organically modified silica nanoparticles as optical probes for cancer cell imaging. Opt Express 16:19568–19578
Rosenholm J, Sahlgren C, Linden M (2010) Towards multi-functional, targeted drug delivery systems using mesoporous silica nanoparticles—opportunities & challenges. Nanoscale 2:1870–1883
Shi H, He X, Yuan Y, Wang K, Liu D (2010) Nanoparticle-based biocompatible and long-life marker for lysosome labeling and tracking. Anal Chem 82:2213–2220
Stöber W, Fink A, Bohn E (1968) Controlled growth of monodisperse silica spheres in the micron size range. J Colloid Interface Sci 26:62–69
Tansub W, Tuitemwong K, Limsuwan P, Theparoonrat S, Tuitemwong P (2012) Synthesis of antibodies-conjugated fluorescent dye-doped silica nanoparticles for a rapid single step detection of *Campylobacter jejuni* in live poultry. J Nanomater 2012:60
Tao G, Chen Q, Yang X, Zhao K, Gao J (2011) Targeting cancer cells through iron(III) complexes of di(picolyl)amine modified silica core–shell nanospheres. Colloids Surf B 86:106–110
van Blaaderen A, Vrij A (1992) Synthesis and characterization of colloidal dispersions of fluorescent, monodisperse silica spheres. Langmuir 8:2921–2931
van Blaaderen A, Vrij A (1993) Synthesis and characterization of monodisperse colloidal organo-silica spheres. Colloid Interface Sci 156:1–18
Watanabe R, Yokoi T, Kobayashi E, Otsuka Y, Shimojima A, Okubo T, Tatsumi T (2011) Extension of size of monodisperse silica nanospheres and their well-ordered assembly. J Colloid Interface Sci 360:1–7
Xia T et al (2009) Polyethyleneimine coating enhances the cellular uptake of mesoporous silica nanoparticles and allows safe delivery of siRNA and DNA constructs. ACS Nano 3:3273–3286
Yokoi T et al (2009) Mechanism of formation of uniform-sized silica nanospheres catalyzed by basic amino acids. Chem Mater 21:3719–3729
Yokoi T, Karouji T, Ohta S, Kondo J, Tatsumi T (2010) Synthesis of mesoporous silica nanospheres promoted by basic

amino acids and their catalytic application. Chem Mater 22:3900–3908

Zhao X, Bagwe R, Tan W (2004) Development of organic-dye-doped silica nanoparticles in a reverse microemulsion. Adv Mater 16:173–176

Zhao B, Yin J, Bilski P, Chignell C, Roberts J, He Y (2009) Enhanced photodynamic efficacy towards melanoma cells by encapsulation of Pc4 in silica nanoparticles. Toxicol Appl Pharmacol 241:163–172